On-Demand Storage of Photonic Qubits at Telecom Wavelengths

Duan-Cheng Liu, Pei-Yun Li, Tian-Xiang Zhu, Liang Zheng, Jian-Yin Huang, Zong-Quan Zhou,* Chuan-Feng Li,† and Guang-Can Guo

CAS Key Laboratory of Quantum Information, University of Science and Technology of China, Hefei 230026, China and CAS Center for Excellence in Quantum Information and Quantum Physics, University of Science and Technology of China, Hefei 230026, China and Hefei National Laboratory, University of Science and Technology of China, Hefei 230088, China

(Received 20 May 2022; accepted 24 October 2022; published 15 November 2022)

Quantum memories at telecom wavelengths are crucial for the construction of large-scale quantum networks based on existing fiber networks. On-demand storage of telecom photonic qubits is an essential request for such networking applications but yet to be demonstrated. Here we demonstrate the storage and on-demand retrieval of telecom photonic qubits using a laser-written waveguide fabricated in an $^{167}Er^{3+}:Y_2SiO_5$ crystal. Both ends of the waveguide memory are directly connected with fiber arrays with a fiber-to-fiber efficiency of 51%. Storage fidelity of 98.3(1)% can be obtained for time-bin qubits encoded with single-photon-level coherent pulses, which is far beyond the maximal fidelity that can be achieved with a classical measure and prepared strategy. This device features high reliability and easy scalability, and it can be directly integrated into fiber networks, which could play an essential role in fiber-based quantum networks.

DOI: 10.1103/PhysRevLett.129.210501

Because of the inevitable photon loss, long-distance quantum communication is a challenging task in fiber networks. A quantum repeater can solve this problem based on quantum memories and entanglement swapping [1]. An elementary link of a quantum repeater, i.e., heralded distribution of two-party entanglements, has been demonstrated using various systems, such as diamond defects [2], trapped ions [3], single atoms [4], quantum dots [5], and atomic ensembles [6,7]. Nevertheless, these systems are not able to provide direct telecom interfaces for fiber networks.

Er^{3+} in solids has highly coherent optical and spin transitions [8,9] and is naturally compatible with the telecom *C* band, which allows long-distance transmission of photons. Significant progress has been made for telecom-wavelength quantum memories using the atomic frequency comb (AFC) protocol [10–15] albeit with predetermined storage times. Storage of classical telecom light with dynamic control can be realized in an on-chip memory device [16]. On-demand storage of weak coherent pulses has been achieved using controlled reversible inhomogeneous broadening protocol [17], while the low achieved efficiency and the resulting low signal-to-noise ratio are insufficient to support storage of qubits. Other than Er^{3+}-doped solids, telecom photons can also be linked with quantum memories by operating with a nondegenerate photon pair source [18,19], quantum frequency conversion [6,20–23], or mechanical resonators [24]. On-demand storage of photonic qubits from external sources is essential for the construction of efficient quantum repeaters based on absorptive quantum memories [1,7,25] but yet to be demonstrated at the telecom wavelengths.

Here we demonstrate a fiber-integrated quantum memory at telecom wavelengths based on a laser-written waveguide fabricated in an $^{167}Er^{3+}:Y_2SiO_5$ crystal. On-demand storage of photonic qubits is achieved with Stark modulation of the AFC storage process using on-chip electrodes [16,26,27]. The experimental setup is illustrated in Fig. 1.

The substrate is an $^{167}Er^{3+}:Y_2SiO_5$ crystal. Y_2SiO_5 is a widely employed host material due to the low magnetic moments of its constituent elements (Y). ^{167}Er is the only stable erbium isotope with nonzero nuclear spin which provides long ground-state population and coherence lifetimes, given that the Er^{3+} electronic spin flips have been inhibited with ultralow temperatures and strong magnetic fields [8,9,28]. To facilitate easy operations, an integrated device with direct fiber connection is preferred for such applications. Among various microfabrication or nanofabrication techniques aimed at integrated quantum memory, femtosecond-laser micromachining (FLM) introduces low damage to substrates and allows three-dimensional fabrication. The storage efficiency of integrated quantum memories in Er-doped crystals are currently limited to 0.2% [13,14], while telecom-wavelength quantum memory has yet to be demonstrated in FLM waveguides.

Here we fabricated a type-III waveguide [29] along the D2 axis in an $^{167}Er^{3+}:Y_2SiO_5$ crystal. The host crystal has a doping level of 50 ppm of $^{167}Er^{3+}$. The symmetric, circular-shaped cross section of a type-III waveguide can support light guidance of arbitrary polarization and facilitates efficient integration with single-mode optical fibers. The fabrication parameters are optimized according to the

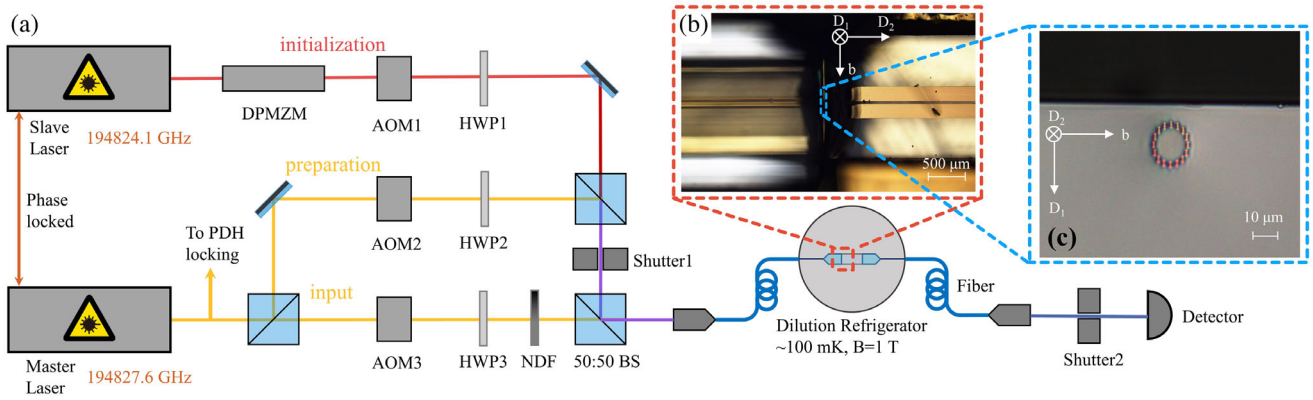

FIG. 1. Diagram of the experimental setup. (a) The optical path before cryostat can be divided into three sections: one for spectral initialization, one for AFC preparation, and one for input pulses. All beams are controlled by acousto-optic modulators (AOM) in double-pass configurations. A dual-parallel Mach-Zehnder modulator (DPMZM) is employed for wideband sweeping during the spectral initialization. The input pulse is attenuated to a weak coherent state by neutral density filters (NDF). All beams are combined with two 50:50 beam splitters and collected into a single-mode fiber connecting to the memory. Polarization of the laser of each beam is adjusted with half wave plates (HWP) to optimize the sample absorption. Two mechanical shutters are employed to protect the single-photon detector from a strong laser. (b) A micrograph of the memory device. On the left is a single-channel fiber array. On the right is the $^{167}Er^{3+}:Y_2SiO_5$ crystal with a laser-written waveguide inside (too thin to be visible) and gold electrodes on top of it. (c) The cross section of the laser-written waveguide.

fiber-coupling efficiency, as discussed in Sec. I of the Supplemental Material [30].

Single-mode fibers were pigtailed at both ends of the waveguide. The contact between the fiber and waveguide is solidified with UV glue. To make the coupling more stable, as shown in Fig. 1(b), the fibers are encapsulated into V-groove assemblies as fiber arrays. A sketch of the fiber-to-waveguide connection is shown in Fig. S1 in the Supplemental Material [30]. The fiber-to-fiber efficiency of this device is 51%, indicating a good matching between the waveguide mode and the fiber mode. Such device efficiency has been comparable to that of commercial fiber-integrated devices such as electro-optic modulators. After mounting into the cryostat, the total efficiency drops to 25% due to additional losses caused by four fiber connectors which can be avoided by fusion splicing of the fibers in future works. A detailed discussion of the total transmission efficiency is given in Sec. V of the Supplemental Material [30].

A pair of gold strip electrodes was placed near both sides of the optical waveguide to apply electric field pulses for the implementation of Stark-modulated AFC storage protocol. Details on the fabrication process are given in Sec. II of the Supplemental Material [30].

Because of the large unquenched electronic angular momenta, Er^{3+} ions in solids are prone to experience spin flips and flip-flops, which will lead to spectral diffusion and short ground-state population lifetimes [35,36], undermining the performances in the storage time and the efficiency. The flip-flops can be reduced when the electronic spins are polarized with a sufficiently low temperature and strong magnetic field [9,28]. Electronic spin flips can be reduced if ultralow temperature is used to directly reduce the phonon density [28], or when a sufficiently strong magnetic field is applied to make most of the phonons off resonant with the electronic Zeeman transition [9]. In this work Er^{3+} ions in site II [37] are addressed, and the magnetic field is applied along the D1 axis of the host crystal for a large electronic Zeeman energy splitting [38]. Here the lowest working temperature is approximately 100 mK, and the magnetic field is 1 T, which is sufficient to create the spectral feature required in this experiment. A higher working temperature can be tolerated if a stronger magnetic field is employed [15].

Our photonic memory is based on the Stark-modulated AFC protocol [16,26,27]. AFC is a periodic spectral profile of an inhomogeneously broadened atomic ensemble [39]. After the AFC absorbs a single photon the quantum state of the atom ensemble undergoes phase evolution according to the transition frequencies of individual atoms. This results in a predetermined photon re-emission at the time of n/Δ where Δ denotes the periodicity of AFC and n represents an arbitrary positive integer. Such phase evolution can be actively controlled by modulating atomic transition frequencies through the linear Stark effect, leading to on-demand retrieval of the signal in discrete steps [16,26,27]. Details on the Stark-modulated AFC protocol and the Stark coefficient are provided in Sec. III of the Supplemental Material [30].

Spectral initialization was performed before AFC preparation to enhance the absorption depth and the storage efficiency. As illustrated in Fig. S3 and detailed in Sec. IV of the Supplemental Material [30], optical pumping was performed roughly in the middle part of the $\Delta m_I = 0$ absorption band to enhance its side parts. Here m_I denotes the quantum number of the nuclear spin. Our electromagnet

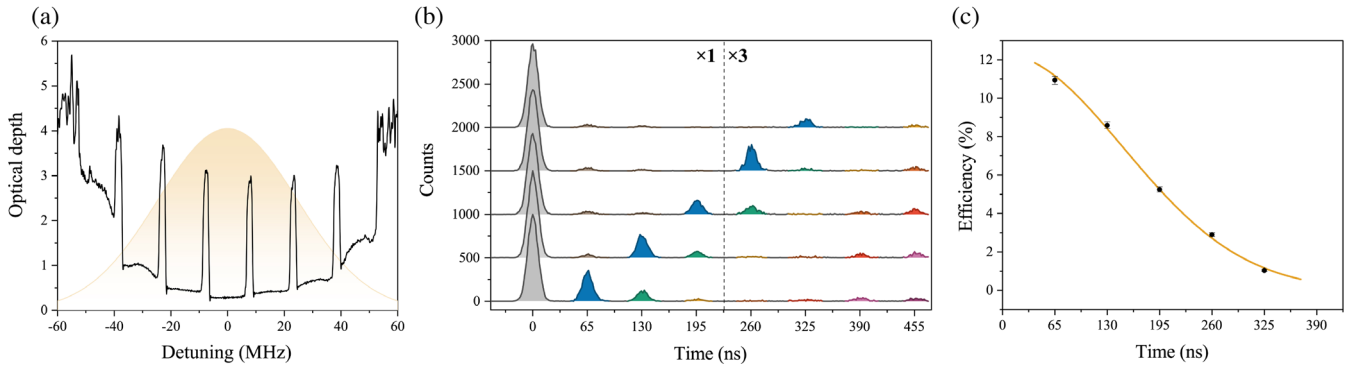

FIG. 2. On-demand storage of single-photon-level inputs. (a) The AFC structure (black line) with a comb spacing of 15.4 MHz and an illustration of the spectral distribution of input pulses (shown in yellow). (b) Photon-counting histogram of on-demand storage with input pulses containing 0.4 photons per pulse on average. Five hundred counts are shifted along the y axis between each set of data. The transmitted input pulses are shown in gray. The on-demand readout echoes are shown in blue. The subsequent emissions are given in other colors. The data after 230 ns are magnified by 3 times for visual convenience. (c) The storage efficiency as a function of readout time. The yellow line is a fit based on Eq. (S2). Here γ is fitted to be 1.8 MHz, which is approximately consistent with the measured AFC structure in Fig. 2(a).

can provide a maximal magnetic field of up to 1 T and in this case the transitions of $\Delta m_I = \pm 1$ and $\Delta m_I = 0$ were not completely resolved in frequency so that the state initialization was performed partially [9,14]. Nevertheless, the spectral initialization process helped to enhance the sample absorption by a magnitude of more than 2 times, which was crucial for high-efficiency storage.

Figure 2(a) presents an example of the prepared AFC which has a bandwidth of 100 MHz and Δ of 15.4 MHz. Figure 2(b) shows the on-demand retrieval of AFC echoes controlled by applying two electric pulses at different times. These electric pulses have a transistor-transistor logic-compatible voltage of ± 4.825 V with the generated electric field of ± 1.2 kV/cm. The pulse duration is set as 18 ns. The input weak coherent state pulse is Gaussian-shaped with a FWHM pulse width of 15 ns and, on average, contains 0.4 photon per pulse. Time dependence of the storage efficiency is presented in Fig. 2(c). The retrieval efficiency is calculated as the AFC echo counts divided by the input pulse counts. The efficiency is $10.9\% \pm 0.2\%$ at a storage time of 65 ns. Compared to previous demonstrations of integrated absorptive telecom quantum memories (including fiber-based ones) [10–14], the storage efficiency has been enhanced by more than 5 times. Because of the low damages introduced by the FLM fabrication and the hyperfine initialization process, the efficiency here is close to the best result reported in bulk crystals [15]. The available absorption depth still set a limit on the achievable storage efficiency, which can be further enhanced through a complete state initialization [9,15] and longer crystals. Storage efficiency toward unity can be obtained by incorporating an impedance-matched optical cavity [40].

To rigorously benchmark the quantum storage performances of this device, we measured the fidelity for storage of time-bin qubits, which are particularly robust in long-distance fiber transmission. A time-bin qubit state of $|e\rangle + e^{i\Delta\alpha}|l\rangle$ was generated with an AOM with a controlled phase $\Delta\alpha$. Each qubit was composed of two 12-ns pulses with a time interval of 40 ns. Four input states of $|e\rangle$, $|l\rangle$, $|e\rangle + i|l\rangle$, and $|e\rangle + e^{i\frac{3}{4}\pi}|l\rangle$ were used to characterize the storage process with a varied average input photon number μ of 0.2, 0.4, 0.8, 1.6, and 3.2. Electric control was configured to on-demand retrieve the signal as the second-order AFC echoes. Here AFC with longer $1/\Delta$ storage times was employed for the storage of time-bin qubits with low crosstalks. Details about the AFC structures employed here are provided in Fig. S5 and Fig. S6 in the Supplemental Material [30].

For $|e\rangle$ and $|l\rangle$, the storage time is 320 ns with an efficiency of $6.9\% \pm 0.1\%$. We obtain average fidelities F_{el} from 98.3% to 99.7% with increased input photon numbers. For superposition states $|e\rangle + i|l\rangle$ and $|e\rangle + e^{i\frac{3}{4}\pi}|l\rangle$, one will need an unbalanced Mach-Zehnder interferometer to project on superposition states. Here we employed a double-AFC architecture [27], which served as a built-in Mach-Zehnder interferometer, to analyze the superposition states. As shown in Fig. 3(a), two AFC structures are superimposed with the $1/\Delta$ storage times of 160 ns and 180 ns, respectively. The relative phase ($\Delta\beta$) between the two paths of such interferometer can be adjusted by shifting the center frequency of one AFC. Projections onto arbitrary superposition states can then be performed. Figures 3(b) and 3(c) show the interference results for input states of $|e\rangle + i|l\rangle$ and $|e\rangle + e^{i3\pi/4}|l\rangle$ with $\mu = 0.8$. Here the fidelity is $F_+ = 97.8\% \pm 0.2\%$ and $F_- = 98.0\% \pm 0.2\%$ for $|e\rangle + i|l\rangle$ and $|e\rangle + e^{i3\pi/4}|l\rangle$, respectively. The average fidelity $F_{+-} = (F_+ + F_-)/2$ is $97.9 \pm 0.2\%$.

The total storage fidelity, as defined by $F_T = \frac{1}{3}F_{el} + \frac{2}{3}F_{+-}$ [41,42,44], is $98.3\% \pm 0.1\%$ for $\mu = 0.8$. This result violates the maximal fidelity (80.9%) that can be achieved by a classical measure-and-prepare strategy [41–43] by

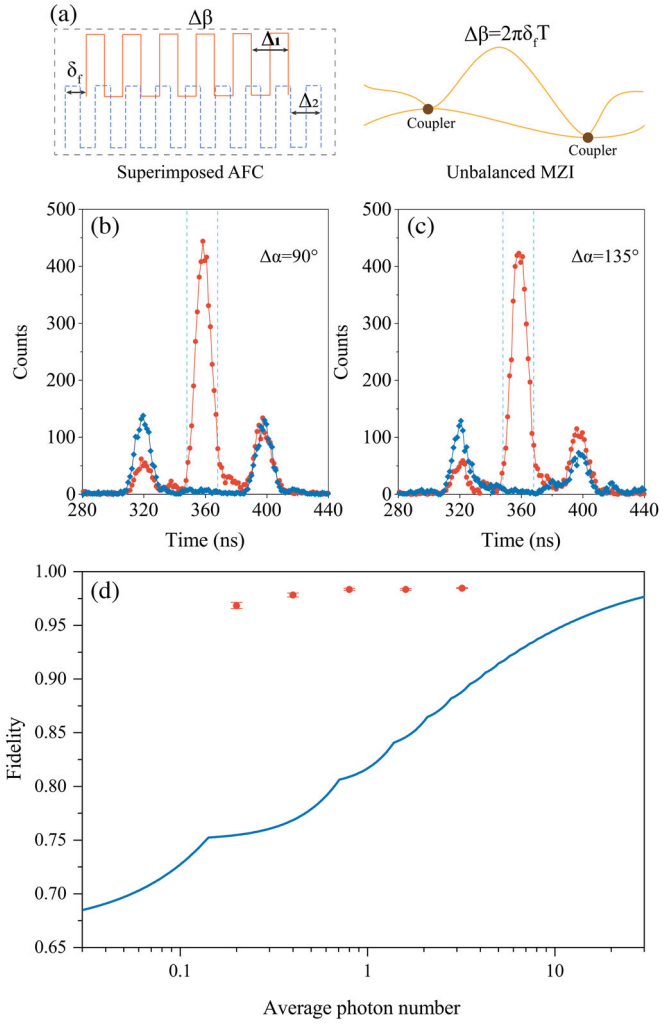

FIG. 3. On-demand storage of time-bin qubits. (a) A pair of superimposed AFCs serves as an unbalanced Mach-Zehnder interferometer (MZI) with adjustable relative phase between two paths. A frequency shift of δ_f for one AFC introduces a phase shift of $\Delta\beta = 2\pi\delta_f T$ where T is the relevant storage time (320 ns). (b), (c) Photon-counting histograms for the constructive (shown in red) and destructive (shown in blue) interference for input states of $|e\rangle + i|l\rangle$ and $|e\rangle + e^{i3\pi/4}|l\rangle$, respectively. Here the average input photon number $\mu = 0.8$. Raw visibility of $95.6\% \pm 0.4\%$ and $96.0\% \pm 0.4\%$ are obtained, respectively. More photon counting histograms are provided in Fig. S6 and Fig. S7 in the Supplemental Material [30]. (d) Total storage fidelity versus the average input photon number per qubit. The red points are experimental results with error bars representing 1 standard deviation. The blue solid line shows the classical bound which takes into account the finite storage efficiency (6.9% for 320 ns) and the Poissonian statistics of the input fields [41–43]. Details on the analysis of storage fidelity are provided in Sec. VII of the Supplemental Material [30].

174 standard deviations, unambiguously demonstrating the reliability of this quantum storage device. Fidelities of various average photon numbers are listed in Table S1 in Supplemental Material [30] and compared with the classical bound in Fig. 3(d). The fidelities with all input levels are far beyond the classical bound. For the lowest input level in our measurements ($\mu = 0.2$), the obtained F_T violates the classical bound by 71 standard deviations. The storage fidelity is not sensitive to the input photon number because of the low noise floor. The unconditional noise probability is $(2.4 \pm 0.5) \times 10^{-4}$ at the detection window. The signal-to-noise ratio is 72 ± 11 when $\mu = 0.2$. The remaining imperfections in fidelity are caused by imperfect measurements, such as the imbalanced storage efficiencies for $|e\rangle$ and $|l\rangle$ with double AFC, and the inaccuracy in the control of $\Delta\beta$.

In conclusion, on-demand storage of telecom photonic qubits is demonstrated in a fiber-integrated quantum memory with high fidelity. Both the fiber arrays and FLM waveguides allow for three-dimensional configurations, which would enable high-density spatial multiplexing for efficient quantum repeaters [1,7]. Substantially longer optical coherence lifetime of $^{167}Er^{3+}:Y_2SiO_5$ can be obtained with larger magnetic fields along preferred orientations where the spectral diffusion effect becomes lower [8,26], so as to enable applications in nonhierarchical quantum repeater architectures [45,46]. For more flexible applications, much longer storage times on the second scale [9] could be obtained with spin-wave storage protocols such as spin-wave AFC [41] or the noiseless photon echo protocol [42]. Our waveguide structure strongly confines the light field so that much larger Rabi frequencies can be obtained [47] to apply the optical π pulses required for spin-wave memories [15]. The close-to-surface optical waveguides can further enable efficient interface with on-chip electric waveguides to facilitate spin decoherence control through dynamical decoupling. With all these developments, the Er-based material can play an essential role in large-scale quantum networks, as it already did in classical fiber networks.

This work is supported by the National Key R&D Program of China (No. 2017YFA0304100), Innovation Program for Quantum Science and Technology (No. 2021ZD0301200), the National Natural Science Foundation of China (No. 12222411 and No. 11821404), and this work was partially carried out at the USTC Center for Micro and Nanoscale Research and Fabrication. Z.-Q. Z acknowledges support from the Youth Innovation Promotion Association CAS.

D.-C. L. and P.-Y. L. contributed equally to this work.

Note added.—During the preparation of this manuscript, we became aware of a related experiment that demonstrates telecom heralded quantum storage in a fiber-integrated laser-written waveguide [48].

*zq_zhou@ustc.edu.cn
†cfli@ustc.edu.cn

[1] N. Sangouard, C. Simon, H. de Riedmatten, and N. Gisin, Quantum repeaters based on atomic ensembles and linear optics, Rev. Mod. Phys. **83**, 33 (2011).

[2] B. Hensen, H. Bernien, A. E. Dréau, A. Reiserer, N. Kalb, M. S. Blok, J. Ruitenberg, R. F. Vermeulen, R. N. Schouten, C. Abellán *et al.*, Loophole-free bell inequality violation using electron spins separated by 1.3 kilometres, Nature (London) **526**, 682 (2015).
[3] D. L. Moehring, P. Maunz, S. Olmschenk, K. C. Younge, D. N. Matsukevich, L.-M. Duan, and C. Monroe, Entanglement of single-atom quantum bits at a distance, Nature (London) **449**, 68 (2007).
[4] J. Hofmann, M. Krug, N. Ortegel, L. Gérard, M. Weber, W. Rosenfeld, and H. Weinfurter, Heralded entanglement between widely separated atoms, Science **337**, 72 (2012).
[5] A. Delteil, Z. Sun, W.-b. Gao, E. Togan, S. Faelt, and A. Imamoğlu, Generation of heralded entanglement between distant hole spins, Nat. Phys. **12**, 218 (2016).
[6] Y. Yu, F. Ma, X.-Y. Luo, B. Jing, P.-F. Sun, R.-Z. Fang, C.-W. Yang, H. Liu, M.-Y. Zheng, X.-P. Xie *et al.*, Entanglement of two quantum memories via fibres over dozens of kilometres, Nature (London) **578**, 240 (2020).
[7] X. Liu, J. Hu, Z.-F. Li, X. Li, P.-Y. Li, P.-J. Liang, Z.-Q. Zhou, C.-F. Li, and G.-C. Guo, Heralded entanglement distribution between two absorptive quantum memories, Nature (London) **594**, 41 (2021).
[8] T. Böttger, C. W. Thiel, R. L. Cone, and Y. Sun, Effects of magnetic field orientation on optical decoherence in $Er^{3+}:Y_2SiO_5$, Phys. Rev. B **79**, 115104 (2009).
[9] M. Rančić, M. P. Hedges, R. L. Ahlefeldt, and M. J. Sellars, Coherence time of over a second in a telecom-compatible quantum memory storage material, Nat. Phys. **14**, 50 (2018).
[10] J. Jin, E. Saglamyurek, Marcel, liGrimau. Puigibert, V. Verma, F. Marsili, S. W. Nam, D. Oblak, and W. Tittel, Telecom-Wavelength Atomic Quantum Memory in Optical Fiber for Heralded Polarization Qubits, Phys. Rev. Lett. **115**, 140501 (2015).
[11] E. Saglamyurek, J. Jin, V. B. Verma, M. D. Shaw, F. Marsili, S. W. Nam, D. Oblak, and W. Tittel, Quantum storage of entangled telecom-wavelength photons in an erbium-doped optical fibre, Nat. Photonics **9**, 83 (2015).
[12] E. Saglamyurek, M. G. Puigibert, Q. Zhou, L. Giner, F. Marsili, V. B. Verma, S. W. Nam, L. Oesterling, D. Nippa, D. Oblak, and W. Tittel, A multiplexed light-matter interface for fibre-based quantum networks, Nat. Commun. **7**, 11202 (2016).
[13] M. F. Askarani, T. Lutz, Marcel, liGrimau. Puigibert, V. B. Verma, M. D. Shaw, S. W. Nam, N. Sinclair, D. Oblak, and W. Tittel, Storage and Reemission of Heralded Telecommunication-Wavelength Photons Using a Crystal Waveguide, Phys. Rev. Appl. **11**, 054056 (2019).
[14] I. Craiciu, M. Lei, J. Rochman, J. M. Kindem, J. G. Bartholomew, E. Miyazono, T. Zhong, N. Sinclair, and A. Faraon, Nanophotonic Quantum Storage at Telecommunication Wavelength, Phys. Rev. Appl. **12**, 024062 (2019).
[15] J. S. Stuart, M. Hedges, R. Ahlefeldt, and M. Sellars, Initialization protocol for efficient quantum memories using resolved hyperfine structure, Phys. Rev. Res. **3**, L032054 (2021).
[16] I. Craiciu, M. Lei, J. Rochman, J. G. Bartholomew, and A. Faraon, Multifunctional on-chip storage at telecommunication wavelength for quantum networks, Optica **8**, 114 (2021).
[17] B. Lauritzen, J. Minář, H. de Riedmatten, M. Afzelius, N. Sangouard, C. Simon, and N. Gisin, Telecommunication-Wavelength Solid-State Memory at the Single Photon Level, Phys. Rev. Lett. **104**, 080502 (2010).
[18] D. Lago-Rivera, S. Grandi, J. V. Rakonjac, A. Seri, and H. de Riedmatten, Telecom-heralded entanglement between multimode solid-state quantum memories, Nature (London) **594**, 37 (2021).
[19] J. V. Rakonjac, D. Lago-Rivera, A. Seri, M. Mazzera, S. Grandi, and H. de Riedmatten, Entanglement between a Telecom Photon and an On-Demand Multimode Solid-State Quantum Memory, Phys. Rev. Lett. **127**, 210502 (2021).
[20] A. Tchebotareva, S. L. N. Hermans, P. C. Humphreys, D. Voigt, P. J. Harmsma, L. K. Cheng, A. L. Verlaan, N. Dijkhuizen, W. de Jong, A. Dréau, and R. Hanson, Entanglement between a Diamond Spin Qubit and a Photonic Time-Bin Qubit at Telecom Wavelength, Phys. Rev. Lett. **123**, 063601 (2019).
[21] T. van Leent, M. Bock, R. Garthoff, K. Redeker, W. Zhang, T. Bauer, W. Rosenfeld, C. Becher, and H. Weinfurter, Long-distance Distribution of Atom-Photon Entanglement at Telecom Wavelength, Phys. Rev. Lett. **124**, 010510 (2020).
[22] T. van Leent, M. Bock, F. Fertig, R. Garthoff, S. Eppelt, Y. Zhou, P. Malik, M. Seubert, T. Bauer, W. Rosenfeld *et al.*, Entangling single atoms over 33 km telecom fibre, Nature (London) **607**, 69 (2022).
[23] M. Bock, P. Eich, S. Kucera, M. Kreis, A. Lenhard, C. Becher, and J. Eschner, High-fidelity entanglement between a trapped ion and a telecom photon via quantum frequency conversion, Nat. Commun. **9**, 1998 (2018).
[24] A. Wallucks, I. Marinković, B. Hensen, R. Stockill, and S. Gröblacher, A quantum memory at telecom wavelengths, Nat. Phys. **16**, 772 (2020).
[25] J.-S. Tang, Z.-Q. Zhou, Y.-T. Wang, Y.-L. Li, X. Liu, Y.-L. Hua, Y. Zou, S. Wang, D.-Y. He, G. Chen *et al.*, Storage of multiple single-photon pulses emitted from a quantum dot in a solid-state quantum memory, Nat. Commun. **6**, 8652 (2015).
[26] S. P. Horvath, M. K. Alqedra, A. Kinos, A. Walther, J. M. Dahlström, S. Kröll, and L. Rippe, Noise-free on-demand atomic frequency comb quantum memory, Phys. Rev. Res. **3**, 023099 (2021).
[27] C. Liu, T.-X. Zhu, M.-X. Su, Y.-Z. Ma, Z.-Q. Zhou, C.-F. Li, and G.-C. Guo, On-Demand Quantum Storage of Photonic Qubits in an On-Chip Waveguide, Phys. Rev. Lett. **125**, 260504 (2020).
[28] J.-Y. Huang, P.-Y. Li, Z.-Q. Zhou, C.-F. Li, and G.-C. Guo, Extending the spin coherence lifetimes of $^{167}Er^{3+}:Y_2SiO_5$ at subkelvin temperatures, Phys. Rev. B **105**, 245134 (2022).
[29] F. Chen and J. V. de Aldana, Optical waveguides in crystalline dielectric materials produced by femtosecond-laser micromachining, Laser Photonics Rev. **8**, 251 (2014).
[30] See Supplemental Material at http://link.aps.org/supplemental/10.1103/PhysRevLett.129.210501 for additional information on the device fabrication, the Stark-modulated AFC protocol, the spectral initialization process, the experimental time sequence and extended

analysis on transmission efficiency and storage fidelity, which includes Refs. [31–34].

[31] R. M. Macfarlane, Optical stark spectroscopy of solids, J. Lumin. **125**, 156 (2007).

[32] M. Izutsu, S. Shikama, and T. Sueta, Integrated optical SSB modulator/frequency shifter, IEEE J. Quantum Electron. **17**, 2225 (1981).

[33] P. Jobez, N. Timoney, C. Laplane, J. Etesse, A. Ferrier, P. Goldner, N. Gisin, and M. Afzelius, Towards highly multimode optical quantum memory for quantum repeaters, Phys. Rev. A **93**, 032327 (2016).

[34] M. Gündoğan, P. M. Ledingham, A. Almasi, M. Cristiani, and H. de Riedmatten, Quantum Storage of a Photonic Polarization Qubit in a Solid, Phys. Rev. Lett. **108**, 190504 (2012).

[35] T. Böttger, C. W. Thiel, Y. Sun, and R. L. Cone, Optical decoherence and spectral diffusion at 1.5 μm in $Er^{3+}:Y_2SiO_5$ versus magnetic field, temperature, and Er^{3+} concentration, Phys. Rev. B **73**, 075101 (2006).

[36] E. Baldit, K. Bencheikh, P. Monnier, S. Briaudeau, J. A. Levenson, V. Crozatier, I. Lorgeré, F. Bretenaker, J. L. Le Gouët, O. Guillot-Noël, and P. Goldner, Identification of λ-like systems in $Er^{3+}:Y_2SiO_5$ and observation of electromagnetically induced transparency, Phys. Rev. B **81**, 144303 (2010).

[37] T. Böttger, C. W. Thiel, Y. Sun, and R. L. Cone, Spectroscopy and dynamics of $Er^{3+}:Y_2SiO_5$ at 1.5 μm, Phys. Rev. B **74**, 075107 (2006).

[38] O. Guillot-Noël, P. Goldner, Y. L. Du, E. Baldit, P. Monnier, and K. Bencheikh, Hyperfine interaction of Er^{3+} ions in Y_2SiO_5: An electron paramagnetic resonance spectroscopy study, Phys. Rev. B **74**, 214409 (2006).

[39] M. Afzelius, C. Simon, H. de Riedmatten, and N. Gisin, Multimode quantum memory based on atomic frequency combs, Phys. Rev. A **79**, 052329 (2009).

[40] M. Sabooni, Q. Li, S. Kröll, and L. Rippe, Efficient Quantum Memory Using a Weakly Absorbing Sample, Phys. Rev. Lett. **110**, 133604 (2013).

[41] M. Gündoğan, P. M. Ledingham, K. Kutluer, M. Mazzera, and H. de Riedmatten, Solid State Spin-Wave Quantum Memory for Time-Bin Qubits, Phys. Rev. Lett. **114**, 230501 (2015).

[42] Y.-Z. Ma, M. Jin, D.-L. Chen, Z.-Q. Zhou, C.-F. Li, and G.-C. Guo, Elimination of noise in optically rephased photon echoes, Nat. Commun. **12**, 4378 (2021).

[43] H. P. Specht, C. Nölleke, A. Reiserer, M. Uphoff, E. Figueroa, S. Ritter, and G. Rempe, A single-atom quantum memory, Nature (London) **473**, 190 (2011).

[44] I. Marcikic, H. De Riedmatten, W. Tittel, H. Zbinden, and N. Gisin, Long-distance teleportation of qubits at telecommunication wavelengths, Nature (London) **421**, 509 (2003).

[45] N. Sinclair, E. Saglamyurek, H. Mallahzadeh, J. A. Slater, M. George, R. Ricken, M. P. Hedges, D. Oblak, C. Simon, W. Sohler, and W. Tittel, Spectral Multiplexing for Scalable Quantum Photonics Using an Atomic Frequency Comb Quantum Memory and Feed-Forward Control, Phys. Rev. Lett. **113**, 053603 (2014).

[46] S. Muralidharan, L. Li, J. Kim, N. Lütkenhaus, M. D. Lukin, and L. Jiang, Optimal architectures for long distance quantum communication, Sci. Rep. **6**, 20463 (2016).

[47] C. Liu, Z.-Q. Zhou, T.-X. Zhu, L. Zheng, M. Jin, X. Liu, P.-Y. Li, J.-Y. Huang, Y. Ma, T. Tu *et al.*, Reliable coherent optical memory based on a laser-written waveguide, Optica **7**, 192 (2020).

[48] J. V. Rakonjac, G. Corrielli, D. Lago-Rivera, A. Seri, M. Mazzera, S. Grandi, R. Osellame, and H. de Riedmatten, Storage and analysis of light-matter entanglement in a fiber-integrated system, Sci. Adv. **8**, eabn3919 (2022).